Chaos in Non Lineal Alfven Waves Using the DNLS Equation

Sergio A. Elaskar, Gonzalo Sánchez-Arriaga and Juan R. Sanmartín

Abstract— **The electro-dynamical tethers emit waves in structured denominated Alfven wings. The Derivative Non-lineal Schrödinger Equation (DNLS) possesses the capacity to describe the propagation of circularly polarized Alfven waves of finite amplitude in cold plasmas. The DNLS equation is truncated to explore the coherent, weakly nonlinear, cubic coupling of three waves near resonance, one wave being linearly unstable and the other waves damped. In this article is presented a theoretical and numerical analysis when the growth rate of the unstable wave is next to zero considering two damping models: Landau and resistive. The DNLS equation presents a chaotic dynamics when is consider only three wave truncation. The evolution to chaos possesses three routes: hard transition, period-doubling and intermittence of type I.**

I. Introduction

The interaction of an electro-dynamical tether with the ionosphere and the terrestrial magnetic field is a source of electromagnetic waves [1-2]. The Alfven waves generated by a conductive body submerged in plasma were predicted by Drell [2] and theses waves were observed for the first time in the Jupiter magnetosphere [3]. An electro-dynamical tether emits waves in structured denominated Alfven wings. It is possible to approach the Alfven wings structure differentiating two regions: 1 - near of the tether (close field), 2 - far away of the tether (distant field). In the close field, the waves have highest intensity and the non-lineal effects are important. The study of the Alfven waves evolution near of the tether can be realized using the Derivative Non-lineal Schrödinger Equation (DNLS). The DNLS equation describes the parallel or almost parallel propagation of the circularly polarized Alfven waves with respect to a non-perturbed magnetic field [4]. This equation has been successful in the understanding of the Alfven waves propagation because numerical simulations and empirical observations, in the space environment, have been explained as the DNLS solutions [5-7].

This work was supported by Ministerio de Ciencia y Tecnología of Spain under Grant ESP2004-01511, by CONICET under Grant PIP 5692, by FONCYT – Universidad Nacional de Rio Cuarto under Grant PICTO-UNRC-2005 Nº 30339, and by Universidad Nacional de Córdoba. under Grant of SECYT.

S. A. Elaskar is with Departamento de Aeronáutica, Universidad Nacional de Córdoba and CONICET, Av. Vélez Sarfield 1611, Córdoba (5000), Argentina, (e-mail: selaskar@efn.uncor.edu).

G. Sanchez-Arriaga is with Escuela Técnica Superior de Ingenieros Aeronáuticos, Universidad Politécnica de Madrid. Plaza Cardenal Cisneros 3, Madrid (28040), España.

J. R. Sanmartín is with Escuela Técnica Superior de Ingenieros Aeronáuticos, Universidad Politécnica de Madrid. Plaza Cardenal Cisneros 3, Madrid (28040), España.

II. DNLS Equation

The DNLS equation can be obtained from two fluid magnetogasdynamics equations considering neutral plasma and rejecting the electrons inertia and the current displacement [8]. If the direction of the magnetic field without perturbing, B_0, is coincident with the z-axis, the DNLS can be expressed in the following form [4,8,9]:

$$\frac{\partial \phi}{\partial t}+\frac{\partial \phi}{\partial z}\pm\frac{i}{2}\frac{\partial^2 \phi}{\partial z^2}+\frac{\partial}{\partial z}\left(\phi\frac{|\phi|^2}{4}\right)+\hat{\gamma}\,\phi=0 \qquad (1)$$

ϕ, t, z represent dimensionless variables and fields: $\phi\equiv\left(B_x\pm i\,B_y\right)/B_0$; $\Omega_i\, z/V_A\rightarrow z$ and $\Omega_i\, t\rightarrow t$. Ω_i is the ionic cyclotron frequency, V_A is the Alfven velocity. The upper and lower signs in Eq.(1) correspond to left and right handed polarized waves (LH and RH) respectively. The last term of Eq.(1) is a damping/growth linear operator [10]. The DNLS equation belongs to the solitones theory and it includes as limits cases the following equations: "Korteweg-Vries, KdV", "Modified Korteweg-Vries, MKdV" and "Non-linear Schrödinger Equation, NLS". DNLS has been analyzed by means of three techniques: search of exact solutions [11], numerical integration [12-13] and reduction to an ordinary differential equations system. This last technique has been carried out in two different ways: supposing stationary travelling waves [14] and by means of a finite number of modes [15-16].

III. Truncation of the DNLS Equation

Because the order of the resulting system depends directly on the modes number, it is important to select the minimum number of waves that reproduces correctly the numerical solutions and empirical data. Numerical integration of the DNLS equation suggests the existence of three dominant modes with a resonance condition [17-18]: $2k_1 = k_2 + k_3$. It is considered, in this work that an approximate solution of the Eq.(1) consists of three travelling waves satisfying the resonance condition:

$$\phi=\sum_{j=1}^{j=3} a_j(t)\, e^{\left[i\psi_j(t)+i(k_j z-\omega_j t)\right]} \qquad (2)$$

a_j, ψ_j are real numbers. The lineal dispersion relation is $\omega_j = k_j \mp k_j^2/2$. Introducing the resonance conditions in Eq.(1) and considering only the components of k_1, k_2 and k_3 (the other components don't possess influence for long times [10]) the following system is obtained [16]:

$$\dot{a}_1=\Gamma a_1- r\, a_1\, a_2^2\, sin\beta \qquad (3a)$$

$$\dot{a}_2=-\gamma_2 a_2+r\, a_2\, a_1^2\, sin\beta \qquad (3b)$$

$$\dot{r}=(\gamma_2-\gamma_3)r+(1-r^2)\, a_1^2\sin\beta \qquad (3c)$$

$$\dot{\beta}=\nu-2a_1^2\left(\bar{V}-\frac{(1+r^2)cos\beta}{2r}\right)-2ra_2^2cos\beta+\frac{a_2^2}{2\bar{V}}\left(\kappa+\frac{r^2}{\kappa}\right) \qquad (3d)$$

with $r = a_2/a_3$, $\bar{V} \equiv (1+\kappa)/2\sqrt{\kappa} > 1$, $\kappa \equiv k_2/k_3 < 1$, $\beta \equiv \pi + \nu t + \psi_2 + \psi_3 - 2\psi_1$, $\gamma_1 \equiv -\Gamma < 0$, $\gamma_2 < \gamma_3$.

The difference of frequencies, $\nu = 2\omega_1 - \omega_2 - \omega_3$, is positive and negative for LH and RH polarization respectively. The Eqs.(3), from the dynamical systems point of view, possess four independent control parameters: Γ, κ, ν and $\delta = \gamma_2/\gamma_3$. However, κ and δ can be related by means of damping models. In this paper are using the Landau and resistive damping models [19].

IV. Atractor for $\Gamma \to 0^+$

The flow divergence for Eqs.(3) is:

$$\frac{\partial}{\partial a_1^2}\frac{da_1^2}{dt} + \frac{\partial}{\partial a_2^2}\frac{da_2^2}{dt} + \frac{\partial}{\partial a_3^2}\frac{da_3^2}{dt} + \frac{\partial}{\partial \beta}\frac{d\beta}{dt} = 2(\Gamma - \gamma_2 - \gamma_3) \tag{4}$$

The flow divergence only presents dependence on the system control parameters. If $(\delta + 1 - \bar{\Gamma}) > 0$ the system is dissipative ($\bar{\Gamma} = \Gamma/\gamma_3$ and $\delta = \gamma_2/\gamma_3$).

The fixed points of the system (3) are defined by:

$$r_p = \kappa; \quad a_{1p}^2 = \frac{\gamma_2}{\kappa \sin\beta_p}; \quad a_{2p}^2 = \frac{\Gamma}{\kappa \sin\beta_p}; \tag{5a}$$

$$\bar{\nu}\sin\beta_p = \alpha - \lambda\cos\beta_p; \quad \bar{\nu} = \nu/\gamma_3 \tag{5b}$$

where: $\alpha = 2\bar{V}\delta^{1/2} - \bar{\Gamma}(\kappa + \delta/\kappa)/(2\bar{V}\delta^{1/2})$; $\lambda = 1 + \delta - 2\bar{\Gamma}$.

Eq.(5b) possesses two solutions: $\cos(\beta_p - \beta^*) = \alpha/\Delta$ and $\cos(\beta^* - \beta_p) = \alpha/\Delta$. The first solution corresponds to the fixed point P* and the second to the fixed point P. The existence of the fixed points should satisfy two requirements: 1 - $\sin\beta_p > 0$; 2 - $|\alpha| \le \left|\sqrt{(\bar{\nu})^2 + \lambda^2}\right|$.

Landau damping

For near parallel propagation the Landau damping is represented by a lineal relation: $\kappa = \delta$ [19]. The fixed point P only exists for LH polarization; the fixed point P* can exist for LH and RH polarization, however P* is unstable. The stability of point P is determined by its characteristic equation, which is a fourth order polynomial. Figure 1 shows the fixed point P stability dominion for $\Gamma \to 0^+$.

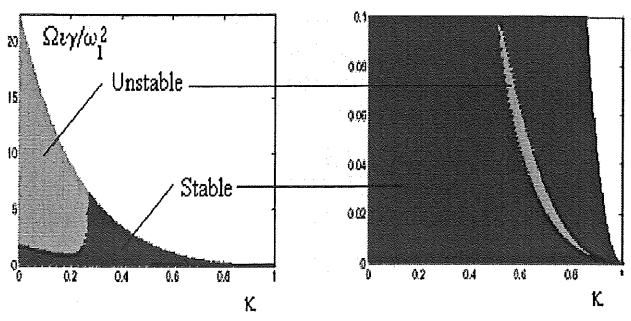

Figure 1a-b. Stability dominion of point P. $\Gamma/\gamma_3 = 0.001$.

When $\Gamma \to 0^+$, the system presents a hard transition to chaos, no matter how small the growth rate of the unstable wave, the four-dimensional flow exhibits chaotic relaxation oscillations that are absent for zero growth-rate [15]. Figure 2 shows the projection on space $\beta - r - a_1$ the fixed point P and the chaotic attractor considering $\nu/\gamma_3 = 1.5$, $\Gamma/\gamma_3 = 0.001$, $\delta = 0.999655012$. This chaotic attractor is placed inside the green zone (Figure 1b). The chaotic behaviour was only found inside of this unstable zone.

To understand the chaotic dynamical behaviour is represented, in Figures 3a-d, the evolution of the maximum a_2 in function of ν for $\Gamma/\gamma_3 = 0.1$ and $\delta = 0.9995$ (bifurcation diagram). The red line corresponds to stable fixed points, the green line to unstable fixed points, the blue line to stable periodic orbits, the black line to unstable periodic orbits, and light blue to chaotic attractors.

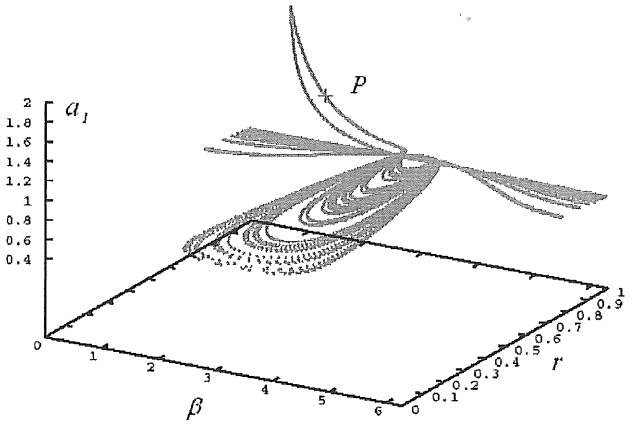

Figure 2. Chaotic attractor projection on space $\beta - r - a_1$. $\Gamma/\gamma_3 = 0.001$, $\delta = 0.999655012$ and $\nu/\gamma_3 = 1.5$.

From Figures 3a-d, one can see a supercritical Hopf bifurcation for $\nu/\gamma_3 \cong 1.227$; a Feigenbaum cascade for $\nu/\gamma_3 \cong 1.67 - 1.68$; a cyclic fold bifurcation and intermittence type I for $\nu/\gamma_3 \cong 1.73$; a new Feigenbaum cascade for $\nu/\gamma_3 \cong 1.82 - 1.89$; a blue sky bifurcation for $\nu/\gamma_3 \cong 2$; a new Hopf supercritical bifurcation for $\nu/\gamma_3 \cong 1.9$; a second cyclic fold bifurcation.

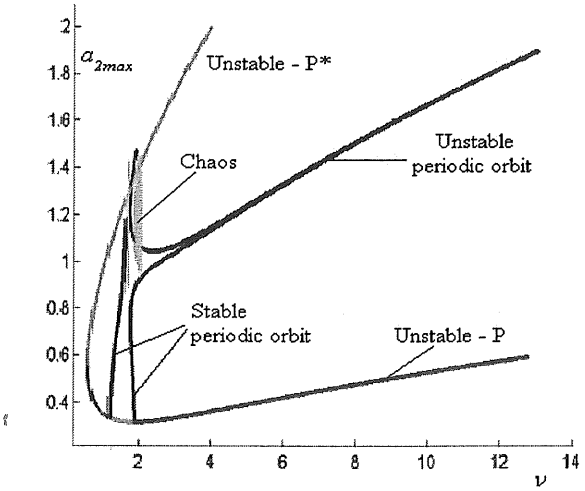

Figure 3a. Bifurcation diagram. $\Gamma/\gamma_3 = 0.1$ and $\delta = 0.9995$.

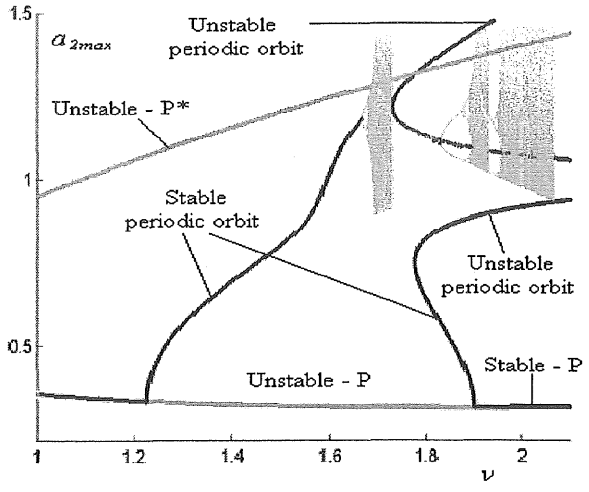

Figure 3b. Bifurcation diagram (zoom). $\Gamma/\gamma_3 = 0.1$ *and* $\delta = 0.9995$.

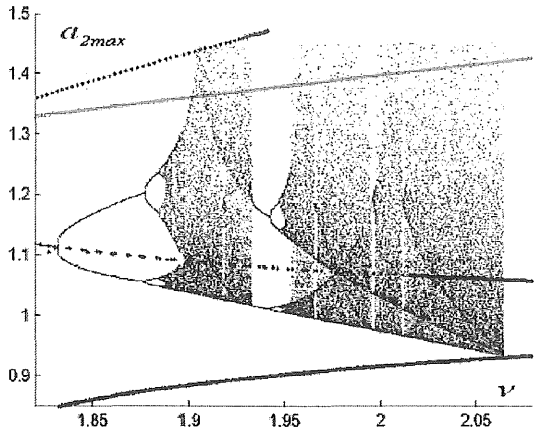

Figure 3d. Bifurcation diagram (zoom). $\Gamma/\gamma_3 = 0.1$ *and* $\delta = 0.9995$ *(zoom).*

Resistive damping

The resistive damping can be represented by the quadratic relation: $\delta = \kappa^2$ [19]. The fixed points are given by Eqs.(5a-b), but the coefficients α, λ are reduced to: $\lambda = 1 + \kappa^2 - 2\overline{\Gamma}$ and $\alpha = 2\overline{V}\kappa - \overline{\Gamma}/\overline{V}$. The fixed points P and P* can exist to LH and RH polarizations. P* is always unstable. The stability analysis for the point P presents some similitude and some difference with regard the Landau damping. The hard transition to chaos, for $\Gamma \to 0^+$ is present; however P is unstable for RH polarizations (Γ/γ_3 = 0.3 and 0.8). Figures 4a-b show the maximum a_2 as function of κ for $\Gamma/\gamma_3 = 0.001$ and ν = 1.5. Figure 4a indicates that P losses its stability for $\kappa \cong 0.82$, next a supercritical Hopf bifurcation appears generating a periodic orbit. For $\kappa \cong 0.9996$ a cyclic fold bifurcation appears and later a Feigenbaum cascade until reaching chaos. In the Figures 4a-c the discontinue manifold was omitted.

Figure 4c shows the maximum a_2 as function of ν/γ_3 for $\Gamma/\gamma_3 = 0.001$ and $\kappa = 0.99995$. For $\nu/\gamma_3 \cong 1.2$ P losses its stability by means of a supercritical Hopf bifurcation, for $\nu/\gamma_3 \cong 1.4$ a cyclic fold bifurcation appears and the chaotic behaviour is generated.

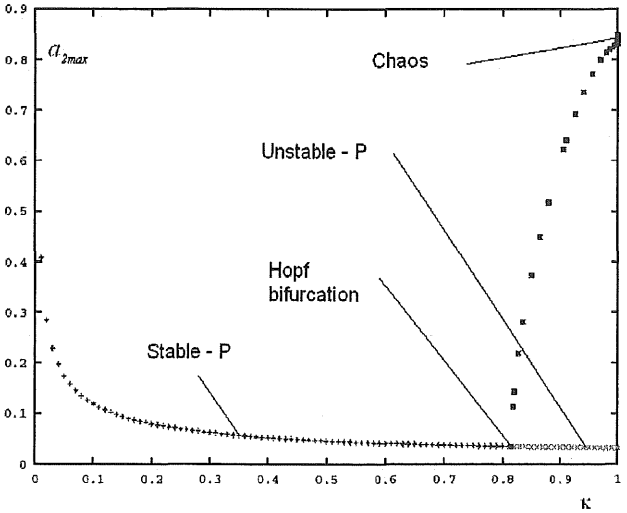

Figure 4a. Bifurcation diagram: maximum a_2 *as function of* κ. *For* $\Gamma/\gamma_3 = 0.001$, $\nu/\gamma_3 = 1.5$.

Figure 5 represents the projection on $\beta - r - a_1$ space of the three 4D-atractors for $\overline{\Gamma} = 0.001$, $\overline{\nu} = 1.5$; and κ = 0.99995 (green); $\kappa = 0.99$ (blue); $\kappa = 0.9$ (red).

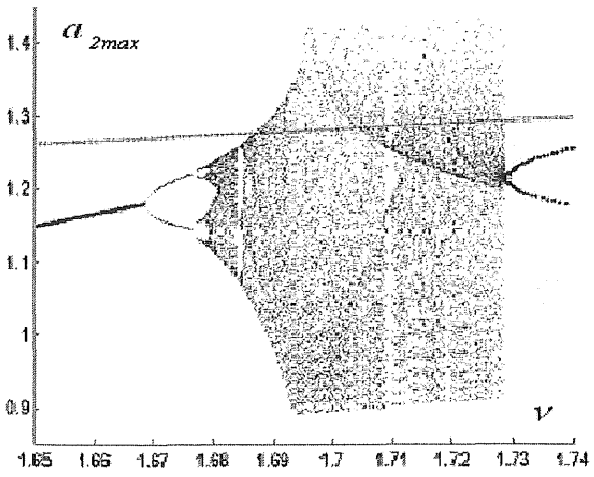

Figure 3c. Bifurcation diagram (zoom). For $\Gamma/\gamma_3 = 0.1$ *and* $\delta = 0.9995$.

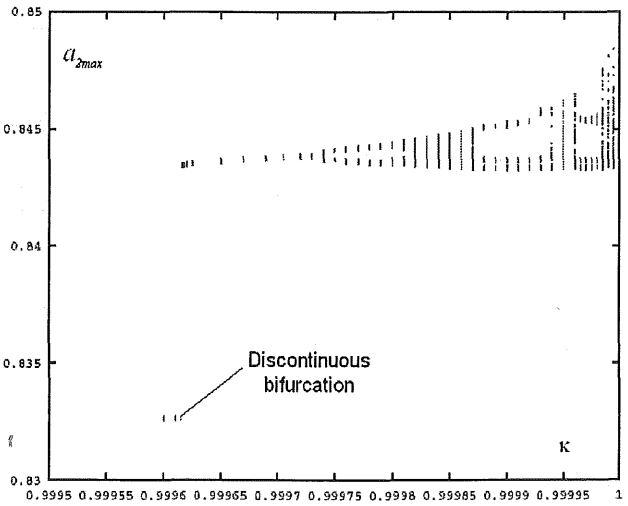

Figure 4b. Bifurcation diagram: maximum a_2 *as function of* κ *(zoom). For* $\Gamma/\gamma_3 = 0.001$, $\nu/\gamma_3 = 1.5$.

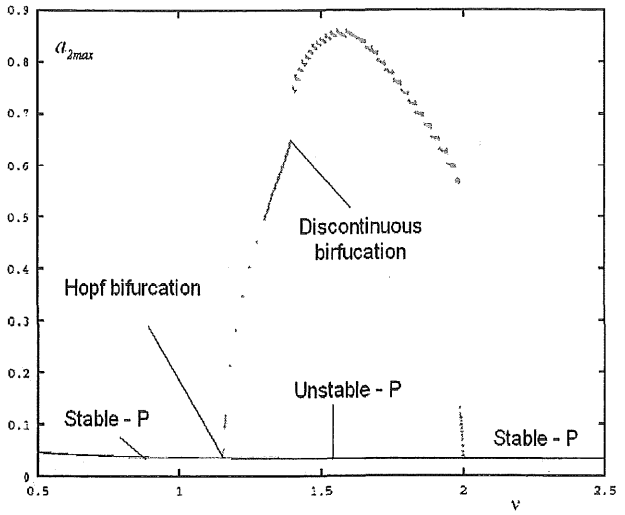

Figure 4c. Bifurcation diagram: maximum a_2 as function of ν/γ_3. $\Gamma/\gamma_3 = 0.001$ and $\kappa = 0.99995$.

Figure 6 represents a bifurcation diagram for $\Gamma/\gamma_3 = 0.2$ and $\nu/\gamma_3 = -10$. Continues lines are unstable periodic orbits. This figure shows a chaotic attractor for RH polarization.

IV. Conclusions

In this work the DNLS equation that describes the propagation and interaction of circularly polarized Alfven waves has been truncated with the purpose of exploring the weakly non-lineal dynamics by means of cubic and coherent interaction of three waves near resonance. One of the waves is lineally unstable and the other two are damped. It was considered two damping models: Landau and resistive.

The system can possess two fixed point: P and P*, being the second of them always unstable. For the Landau damping the point P doesn't exist for RH polarization. For resistive damping P exists for LH and RH polarizations. It is important to note that P is unstable inside of certain parametric domain, including RH polarizations.

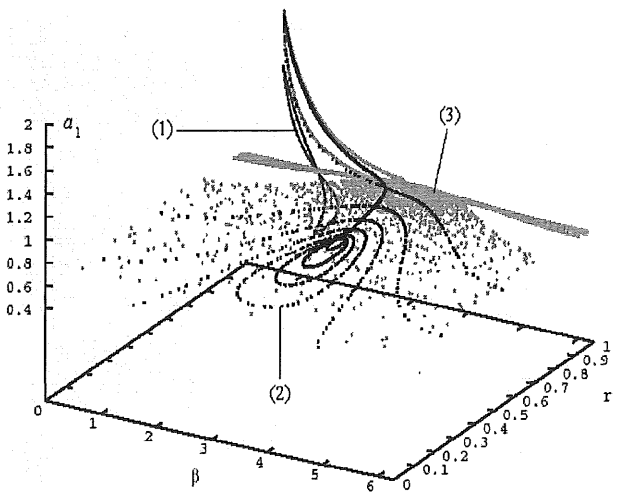

Figure 5. 4D-atractors projection on space $\beta - r - a_1$ corresponding to: (1) $\kappa = 0.9$ – (2) $\kappa = 0.99$ – (3) $\kappa = 0.99995$. For $\bar{\Gamma} = 0.001$, $\bar{\nu} = 1.5$.

The DNLS equation, with RH polarization, can present a chaotic dynamics considering only three wave interaction, this results is important because previous work established necessary seven waves [17].

The evolution to chaos possesses three routes depending of the parameter considered: hard transition, period-doubling and intermittence of type I. The two first were obtained in previous works [15-16], however the intermittency type I is a new result.

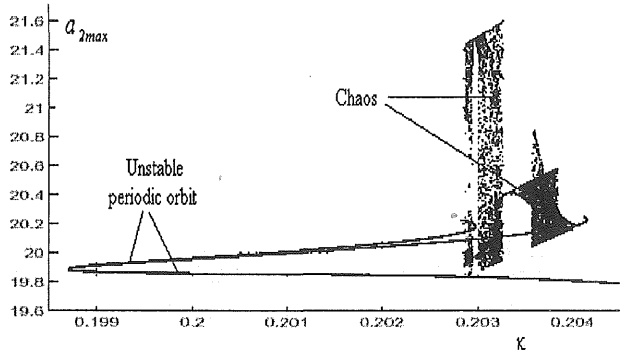

Figure 6. Chaotic attractor. $\Gamma/\gamma_3 = 0.2$ and $\nu/\gamma_3 = -10$

References

[1] M. Dobrowolny and E. Melchioni. Electrodynamic aspects of the thrust tethered satellite mission. *J. Geophys. Res.*, 98(13): 761 (1993).

[2] S. Drell, H. Foley and M. Ruderman. Drag and propulsion of large satellites in the ionosphere: An Alfvén propulsion engine in space. *J. Geophys. Res.*, 70: 3131, 1965.

[3] M. Acuna and F. Ness. Standing Alfven wave current system at Io:Voyager I Observations. *J. Geophys. Res.*, 86: 8513, 1981.

[4] A. Rogister. Parallel Propagation of Nonlinear Low-Frequency Waves in High-β Plasma. *The Physics of Fluids*, 14(12): 2733-2739, 1971.

[5] E. J. Smith, A. Balogh, M. Neugebauer and D. McComas. Ulysses Observations of Alfvén waves in the Southern and Northhern Hemispheres. *Geophys Res. Lett.*, 22: 3381, 1995.

[6] E. Marsch and S. Liu. Structure Functions and Intermittency of Velocity Fluctuations in the Inner Solar Wind. *Ann. Geophys.*, 11:227, 1993.

[7] R. Bruno, V. Carbone, P. Veltri, E. Pietropaolo, B. Bavassano. Identifying intermittency events in the solar wind. *Planetary and Space Science.* 49: 1201-1210, 2001.

[8] E. Mjølhus. On the modulational instability of hydromagnetic waves parallel to the magnetic field. *J. Plasma Phys.* 16: 321-334, 1976.

[9] T. Passot and P. Sulem, Long-Alfvén-wave trains in collisionless plasmas. I. Kinetic theory. *Phys. Plasmas* 10:3887-3905, 2003.

[10] D. Russell and E. Ott. Chaotic (strange) and periodic behaviour in instability saturation by the oscillating two stream instability, *Phys. Fluids*, 24: 1976-1988, 1981.

[11] E. Mjolhus and T. Hada, *Nonlinear Waves and Chaos in Space Plasmas*, edited by T. Hada and H. Matsumoto (Terrapub, Tokio), 121-169, 1997.

[12] S. Splanger, J. Sheerin and G. Payne. A numerical study of nonlinear Alfvén waves and solitons. *Phys Fluids*, 28: 104-109, 1985.

[13] S. Dawson and C. Fontan. Soliton decay of nonlinear Alfvén waves: Numerical studies. *Phys. Fluids*, 31(1): 83-89, 1988.

[14] T. Hada, C. Kennek, B. Buti and E. Mjolhus. Chaos in driven Alfvén systems. *Phys. Fluids* B2(11): 2581-2590, 1990.

[15] J. Sanmartín, O. López-Rebollal, E. del Río and S. Elaskar. Hard transition to chaotic dynamics in Alfvén wave-fronts. *Physics of Plasmas*, 11(5): 2026-2035, 2004.

[16] S. Elaskar, G. Sanchez-Arriaga and J. Sanmartín. Fully three wave model to study the hard transition to chaotic dynamics in Alfvén wave fronts. *Mecánica Computacional*, 24: 2271-2288, 2005.

[17] S. Ghosh and K. Papadopoulos. The onset of Alfvenic turbulence. *Phys. Fluids*, 30: 1371-1387, 1987.

[18] Y. Nariyuki and T. Hada. Self-generation of phase coherence in parallel Alfvén turbulence. *Earth Planets Sapce*, 57: 9-12, 2005.

[19] A. Akhiezer, I. Akhiezer, R. Polovin, A. Sitenko and K. Stepanov. *Plasma Electrodynamics.* Vol 1. Pergamon, New York, 1975.